



ELSEVIER

Contents lists available at ScienceDirect

# Applied Radiation and Isotopes

journal homepage: [www.elsevier.com/locate/apradiso](http://www.elsevier.com/locate/apradiso)

## Gamma-ray spectrometry in the decay of $^{194}\text{Ir}$ to $^{194}\text{Pt}$



K.S. Krane

Department of Physics, Oregon State University, Corvallis, OR 97331, USA

### HIGHLIGHTS

- The decay of  $^{194}\text{Ir}$  was studied with high-resolution gamma-ray spectrometry.
- Energy and intensity precisions have been improved for 64 gamma rays.
- Three gamma rays previously unknown in the Ir decay were observed.
- Good agreement was obtained with the corresponding gamma rays from the  $^{194}\text{Au}$  decay.
- Energies and beta intensities were deduced for the  $^{194}\text{Pt}$  levels.

### ARTICLE INFO

#### Article history:

Received 28 January 2016

Received in revised form

31 May 2016

Accepted 7 June 2016

Available online 8 June 2016

#### Keywords:

 $^{194}\text{Ir}$  decay

Gamma-ray spectrometry

 $^{194}\text{Pt}$  energy levels

### ABSTRACT

As a complement to a recent high-resolution spectrometric investigation of the decay of  $^{194}\text{Au}$  to levels of  $^{194}\text{Pt}$ , a similar study has been undertaken of the decay of 19-h  $^{194}\text{Ir}$  to  $^{194}\text{Pt}$ . The two decays populate a similar set of levels in  $^{194}\text{Pt}$ , and so the complementary investigations with similar resolution and efficiency permit a direct comparison of the two data sets. Overall there is excellent agreement between the energies of the common  $\gamma$ -ray transitions and also between the deduced energies of the excited states in  $^{194}\text{Pt}$ . The  $^{194}\text{Ir}$  half-life has been remeasured to be 19.20(2) h.

© 2016 Elsevier Ltd. All rights reserved.

### 1. Introduction

A recent publication (Dorsett and Krane, 2015) described a study of the decay of  $^{194}\text{Au}$  (produced following the decay of 447-y  $^{194}\text{Hg}$ ) to levels in  $^{194}\text{Pt}$  by observing the emitted  $\gamma$  radiations with high-resolution counting systems. In all about 200 transitions have been placed among nearly 50 excited states in  $^{194}\text{Pt}$ . The detailed spectrometric study of this decay was facilitated by the large  $Q$ -value of the decay (2.5 MeV), which resulted in the population of many excited states, as well as by the long half-life of the parent, which permitted long counting periods that revealed the presence of very weak transitions (with relative intensities smaller than  $10^{-4}$ ).

The  $\beta^-$  decay of  $^{194}\text{Ir}$  to  $^{194}\text{Pt}$  is in many ways similar to the electron capture and  $\beta^+$  decay of  $^{194}\text{Au}$ . The  $Q$ -values are similar (respectively 2.2 and 2.5 MeV) and the spin-parities are identical ( $1^-$ ), so many of the same excited states are populated. There are, however, two principal differences between the decays: the half-life of  $^{194}\text{Ir}$  is 19 h (vs. 447 y for the parent of  $^{194}\text{Au}$ ), which limits the amount of data that can be obtained from a single counting sample, and 95% the  $^{194}\text{Ir}$   $\beta$ -decay intensity populates the ground and first excited state (vs. 54% for the  $^{194}\text{Au}$  decay), so the states above the first excited state receive only 5% of the decay intensity

in  $^{194}\text{Ir}$  compared with 46% in  $^{194}\text{Au}$  and thus for each  $\beta$  decay of the parent Au produces about 10 times as much upper-level  $\gamma$  ray intensity as Ir.

Despite these restrictions, a high-resolution spectrometric study of the  $^{194}\text{Ir}$  can produce a set of  $\gamma$ -ray energies and intensities of quality and precision approaching that of the  $^{194}\text{Au}$  decay. The present work presents these results along with a comparison of the resulting conclusions for the level structure of  $^{194}\text{Pt}$ .

### 2. Experimental details

Radioactive samples of  $^{194}\text{Ir}$  were produced by neutron irradiation of Ir in the Oregon State University TRIGA reactor. Three different source materials were used: Ir metal powder and a spectroscopically pure dilute ( $1 \mu\text{g}$  per  $\mu\text{L}$ ) solution of  $\text{IrCl}_3$  in HCl, both of natural isotopic abundance (62.7%  $^{193}\text{Ir}$  and 37.3%  $^{191}\text{Ir}$ ), and Ir metal powder enriched to 98.5% in  $^{193}\text{Ir}$  (the remaining 1.5% being  $^{191}\text{Ir}$ ). The irradiation of the natural Ir produced samples that were initially about 98% 19-h  $^{194}\text{Ir}$  and 2% 74-d  $^{192}\text{Ir}$ , while the irradiated enriched samples were initially 99.9%  $^{194}\text{Ir}$  and 0.1%  $^{192}\text{Ir}$ . Following the irradiations the activity of the nonenriched samples

was about 4 MBq while that of the enriched samples was about 2 MBq. The samples were counted over 5–7 days and were gradually moved closer to the detectors as the activity decreased, beginning at 20–28 cm and ending at 5–10 cm. Source strengths were adjusted so as to keep the dead time of the counting system at around 20%, in part to compensate for the reduced intensity of the emitted  $\gamma$  radiations compared with the  $^{194}\text{Hg}$  source, for which the counting dead times were more typically 5%.

The  $\gamma$  rays were observed with high-resolution Ge detectors (efficiency of 35–40% compared with NaI at 1332 keV, resolution of 1.7–1.8 keV at 1332 keV) connected to a computer-based, gain-stabilized DSPEC digital signal processor (<http://www.ortec-online.com/>). Efficiency calibrations were done with sources of  $^{133}\text{Ba}$  and  $^{152}\text{Eu}$  using intensities given by Bé et al. (2006). Below 200 keV, the determination of relative efficiency was augmented using sources of  $^{160}\text{Tb}$ ,  $^{169}\text{Yb}$ , and  $^{182}\text{Ta}$ . This gave a total of 36 data points below 444 keV, which were fit using a 4th order polynomial for the log-log relationship between efficiency and energy. Above 444 keV the logarithmic dependence is well fit with a linear function. Corrections for high-energy efficiencies (above 1.4 MeV) were made using a source of  $^{56}\text{Co}$ . Uncertainties in the relative efficiencies were set at no smaller than 2% for energies below 250 keV and 1% for energies above 250 keV.

Energy calibrations were accomplished through simultaneous measurements of the Ir samples with samples of  $^{24}\text{Na}$ ,  $^{56}\text{Mn}$ ,  $^{133}\text{Ba}$ ,  $^{152}\text{Eu}$ , and  $^{207}\text{Bi}$  in various combinations. In addition, the  $^{192}\text{Ir}$  present in the samples served as energy calibration. Energy values of the calibration lines were taken from Helmer and van der Leun (2000) and Bé et al. (2006). Some spectra were accumulated without external sources, in which case the stronger  $^{194}\text{Ir}$  lines

served as secondary calibration standards. Even though uncertainties of many of the external calibration lines are smaller than 10 eV, so that even in combination with the statistical and fitting uncertainties the net uncertainty would often fall below 10 eV, the minimum energy uncertainty has been set at 10 eV for Ir lines compared directly with the primary calibration standards, with correspondingly larger minima for weaker lines calibrated against the secondary Ir standards. The spectra were analyzed using the peak-fitting code SAMPO (Aarnio et al., 1988) to determine energies and intensities.

In all 15 spectra were accumulated, 5 from each of the 3 samples (2 non-enriched, 1 enriched) at source-to-detector distances ranging from 5 to 28 cm. Each spectrum was individually energy calibrated as described above, and in each spectrum the peak intensities were corrected for detector efficiency at the appropriate counting geometry and normalized to the intensity of the 328 keV line (which was set at 100 units). Data from the 15 spectra were combined by taking either the unweighted average of values at or close to the minimum uncertainties (1% or 2% for intensities, 10 eV for energies) with no reduction in the uncertainty of the final result, or the weighted average of the individual values with larger uncertainties (but in no case allowing the uncertainty of the average to fall below the assumed minima).

### 3. Results

Figs. 1 and 2 show the low-energy and high-energy portions of the spectrum of a liquid Ir sample (hence the presence of the two  $^{38}\text{Cl}$  lines). In the spectra of the enriched sample, the  $^{192}\text{Ir}$  lines are

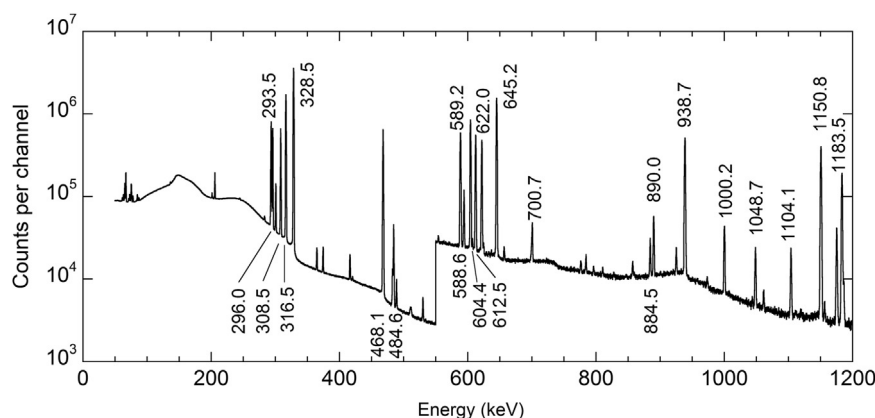


Fig. 1. Low-energy portion of  $\gamma$ -ray spectrum from  $^{194}\text{Ir}$  source. Energy labels above the spectrum mark the most intense  $^{194}\text{Ir}$  lines; labels below the spectrum mark the  $^{192}\text{Ir}$  lines.

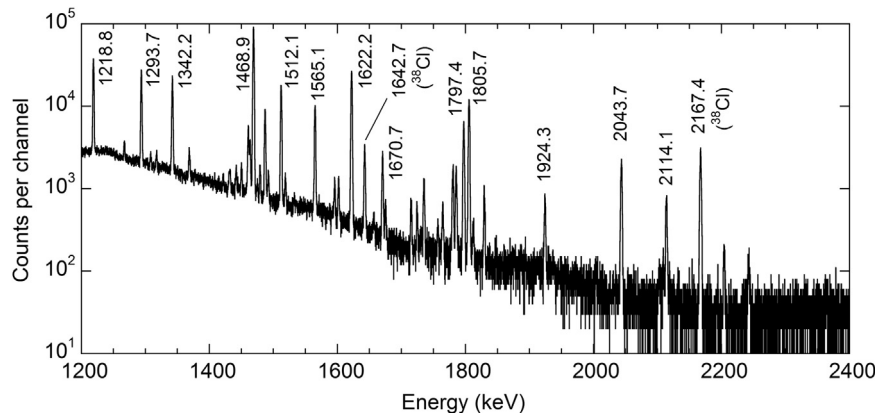


Fig. 2. High-energy portion of  $\gamma$ -ray spectrum from  $^{194}\text{Ir}$  source.

Download English Version:

<https://daneshyari.com/en/article/8209128>

Download Persian Version:

<https://daneshyari.com/article/8209128>

[Daneshyari.com](https://daneshyari.com)